

## Article

# From Structure to Luminescent Properties of $B_2O_3$ - $Bi_2O_3$ - $SrF_2$ Glass and Glass-Ceramics Doped with $Eu^{3+}$ Ions

Karolina Milewska <sup>1,\*</sup>, Michał Maciejewski <sup>1</sup>, Anna Synak <sup>2</sup>, Marcin Łapiński <sup>1</sup>,  
Aleksandra Mielewczyk-Gryń <sup>1</sup>, Wojciech Sadowski <sup>1</sup> and Barbara Kościelna <sup>1,\*</sup>

<sup>1</sup> Faculty of Applied Physics and Mathematics, Institute of Nanotechnology and Materials Engineering, Gdańsk University of Technology, ul. Gabriela Narutowicza 11/12, 80-233 Gdańsk, Poland; michal.maciejewski@pg.edu.pl (M.M.); marcin.lapinski@pg.edu.pl (M.L.); alegryn@pg.edu.pl (A.M.-G.); wojciech.sadowski@pg.edu.pl (W.S.)

<sup>2</sup> Faculty of Mathematics, Physics and Informatics, Institute of Experimental Physics, University of Gdańsk, ul. Wita Stwosza 57/246, 80-952 Gdańsk, Poland; anna.synak@ug.edu.pl

\* Correspondence: karolina.milewska@pg.edu.pl (K.M.); barbara.koscielna@pg.edu.pl (B.K.)

**Abstract:** Glass-ceramics with the composition  $B_2O_3$ - $Bi_2O_3$ - $SrF_2$  were synthesized by the conventional melt-quenching technique and subsequent crystallization of the parental glasses. The temperature at which the ceramization was carried out was selected based on differential scanning calorimetry (DSC) analysis. The structure of the studied materials and the formation of  $SrF_2$  nanocrystals were confirmed by the Fourier-transform infrared spectroscopy (FTIR), X-ray diffraction (XRD), and X-ray photoelectron spectroscopy (XPS) techniques. It was found that the amount of strontium fluoride introduced into the parental borate-bismuth glass has a significant impact on the growth of  $SrF_2$  nanocrystals. In particular, the influence of the crystalline  $SrF_2$  phase on luminescence intensity and kinetics was studied using  $Eu_2O_3$ -doped samples. An increase in luminescence intensity was observed in the samples in which  $SrF_2$  nanocrystals were formed. This is most likely related to the fact that some of the  $Eu^{3+}$  ions were (after annealing of the glass) located in the crystalline structure of strontium fluoride. This was confirmed both by the luminescence lifetime obtained based on the luminescence decay curves and the calculated Judd–Ofelt parameters,  $\Omega_2$  and  $\Omega_4$ . The results achieved confirm that the glasses and glass-ceramics described in this work could be considered as a new phosphor for light-emitting diodes (LEDs).

**Keywords:** glass; glass-ceramics; luminescence; nanocrystals



**Citation:** Milewska, K.; Maciejewski, M.; Synak, A.; Łapiński, M.; Mielewczyk-Gryń, A.; Sadowski, W.; Kościelna, B. From Structure to Luminescent Properties of  $B_2O_3$ - $Bi_2O_3$ - $SrF_2$  Glass and Glass-Ceramics Doped with  $Eu^{3+}$  Ions. *Materials* **2021**, *14*, 4490. <https://doi.org/10.3390/ma14164490>

Academic Editor: Gregorio Bottaro

Received: 30 June 2021

Accepted: 7 August 2021

Published: 10 August 2021

**Publisher's Note:** MDPI stays neutral with regard to jurisdictional claims in published maps and institutional affiliations.



**Copyright:** © 2021 by the authors. Licensee MDPI, Basel, Switzerland. This article is an open access article distributed under the terms and conditions of the Creative Commons Attribution (CC BY) license (<https://creativecommons.org/licenses/by/4.0/>).

## 1. Introduction

Glass as a material for applications in optics and optoelectronics has enjoyed unflagging interest for many years. In particular, a lot of research is related to glasses and glass-ceramics with optically active dopants such as rare-earth ions, which are promising materials for use in white LEDs [1–3]. This is because of their unique combination of properties for excellent transmission in the visible and infrared spectral range, high refractive index, and good chemical and mechanical stability [4,5]. Glasses that are the matrix for the rare-earth ions should also have low phonon energy, which decreases the risk of multi-phonon relaxation processes and, consequently, of non-radiative transitions [6]. When we consider glasses for these applications, borate glasses seem to have great potential. Boron oxide as a glass former is characterized by a wide glass formation range, high transparency, and high thermal stability [7]. Unfortunately, the addition of some network modifiers to boron oxide, usually alkali oxides, can lead to a change of coordination number of some of the boron atoms from 3 to 4, changing the properties of borate glass. Interestingly, the property change does not occur linearly with the amount of modifier. This phenomenon is known as the borate anomaly [8–10]. The modifier that allows very good optical properties of borate glasses to be obtained is bismuth oxide. Borate-bismuth

glasses are characterized by high density and high refractive indices and, importantly due to their preparation, are glasses with a comparatively low melting point in a wide glass formation range (20–80 mol %  $\text{Bi}_2\text{O}_3$ ) [11]. The choice of bismuth oxide over lead oxide, which has often been used in glasses in recent years, seems particularly good, as it breaks down the toxic material while leaving the glass with the desired properties. However, the addition of  $\text{Bi}_2\text{O}_3$  to borate oxide also changes the coordination number of the boron atoms [10,12,13], changing the properties of the resulting glass.

Borate glasses were often used as matrices for  $\text{RE}^{3+}$  ions [12,14,15]. However, research devoted to this subject has shown that an interesting alternative to glasses are glass-ceramics, especially those containing metal fluoride nanocrystals. Optical transparency of glass-ceramics can be reached if the crystallite diameter does not exceed 30 nm [16]. Crystal lattice, especially when the crystalline phase is fluoride, prevents them from luminescence concentration quenching due to clusters of  $\text{RE}^{3+}$  ions forming [17–19]. Furthermore, if there are heavy atoms in the structure of the nanocrystals, an additional factor appears in the amorphous matrix that reduces the phonon energy of the matrix what consequently promotes  $\text{RE}^{3+}$  radiative transitions, keeping all the benefits of the glass matrix at the same time [17,20–23]. Much research has been related to the existence of  $\text{PbF}_2$  nanocrystals in the borate matrix [14,15]. However, as mentioned earlier, lead is being phased out due to its toxicity. Among various fluoride nanocrystals, which are more environmentally friendly than lead compounds, strontium fluoride  $\text{SrF}_2$  seems to be a very good choice in terms of materials for optical applications. This is because  $\text{SrF}_2$  exhibits a wide bandgap, low phonon energy, and relatively low hygroscopic properties [24]. On the other hand, to the best of our knowledge, there is no information in the literature on the possibility of crystallization of  $\text{SrF}_2$  in a borate-bismuth matrix.  $\text{SrF}_2$  nanocrystals are usually grown in glasses by annealing them at a suitable temperature above the glass transition temperature ( $T_g$ ). The size of nanocrystals can be then controlled by changing heat treatment parameters, but it also depends on the type of glass structure [23–27]. In the case of borate-bismuth glass, the problem is more complicated because in this glass it is possible to obtain at least five stable crystalline phases of  $\text{Bi}_2\text{O}_3$ - $\text{B}_2\text{O}_3$  [11] and metastable bismuth orthoborate phases [28]. They can also crystallize in the matrix during annealing, leading to the crystallization of the  $\text{SrF}_2$  phase. Nevertheless, due to the optical properties of borane-bismuth glasses and the known beneficial effect of  $\text{SrF}_2$  nanocrystals on the luminescence of rare-earth ions, it is worth undertaking such research.

This work is devoted to the synthesis of borate-bismuth glasses and glass-ceramics containing  $\text{SrF}_2$  nanocrystals. We present here the results of structural studies of the above materials, as well as the impact of annealing the glasses on the luminescent properties of  $\text{Eu}^{3+}$  ions incorporated in them. The research was carried out to assess these materials as potential candidates for LED phosphors.

## 2. Materials and Methods

Borate-bismuth glasses with a nominal composition (in mol%) of  $50\text{B}_2\text{O}_3$ - $50\text{Bi}_2\text{O}_3$  (BBO),  $45\text{B}_2\text{O}_3$ - $45\text{Bi}_2\text{O}_3$ - $10\text{SrF}_2$  (BBO+ $10\text{SrF}_2$ ), and  $40\text{B}_2\text{O}_3$ - $40\text{Bi}_2\text{O}_3$ - $20\text{SrF}_2$  (BBO+ $20\text{SrF}_2$ ) were synthesized using the conventional melt quenching technique. Moreover, glasses doped with  $\text{Eu}_2\text{O}_3$  (2 mol %) were prepared: BBO+Eu, BBO+ $10\text{SrF}_2$ +Eu, and BBO+ $20\text{SrF}_2$ +Eu. Well-mixed starting raw materials  $\text{H}_3\text{BO}_3$ ,  $\text{Bi}_5\text{OH}(\text{OH})_9(\text{NO}_3)_4$ ,  $\text{SrF}_2$ , and  $\text{Eu}(\text{NO}_3)_3$  were melted in a porcelain crucible at  $1100\text{ }^\circ\text{C}$  for 15 min. After that, melts were poured onto a steel hot plate ( $\sim 250\text{ }^\circ\text{C}$ ) and immediately pressed by another plate, and then cooled down to room temperature. To investigate the effect of annealing the glasses on the crystallization of  $\text{SrF}_2$  nanocrystals, the samples were annealed in the interval of  $450$ – $590\text{ }^\circ\text{C}$  for 1 h and 24 h in an air atmosphere.

Thermal properties of as-prepared glasses were studied on a Netzsch Simultaneous Thermal Analyzer, STA 449 F1, in the platinum-rhodium crucible in an air atmosphere, with a heating rate of 10 K/min. Before each measurement, a blank calibration run was conducted to account for the buoyancy effect. Differential scanning calorimetry (DSC)

allowed the characteristic temperatures to be determined, such as the glass transition temperature  $T_g$  and crystallization temperature  $T_c$ .

The amorphous nature of the glasses as well as the presence of crystalline phases present in them as a result of annealing was confirmed in X-ray diffraction (XRD) studies. XRD measurements were performed on powder samples on a Philips X'PERT PLUS diffractometer with Cu-K $\alpha$  radiation.

To determinate the types of structural units present in the samples, Fourier transform infrared spectroscopy (FTIR) measurements were carried out. The measurements were performed on a Perkin-Elmer Frontier MIR/FIR spectrometer with a TGS detector on pellet samples mixed with potassium bromide KBr in a weight ratio (Sample:KBr) of 1:100.

X-ray photoelectron spectroscopy (XPS) analysis confirming the valence states of ions present in the samples was carried out with an Omnicron NanoTechnology spectrometer with a 128-channel collector. XPS measurements were performed in ultra-high vacuum conditions, below  $1.1 \times 10^{-8}$  mBar. The photoelectrons were excited by an Mg-K $\alpha$  X-ray source with X-ray anode operated at 15 keV and 300 W.

Luminescence emission and excitation spectra of the samples were collected by a SCINCO FluoroMate FS-2 fluorescence spectrometer using pellet samples mixed with KBr in a weight ratio of 1:1. The single measurement results were obtained as a quasi-three-dimensional, colorful flat image, with the wavelength in the horizontal axis, the time in the vertical axis, and the intensity expressed by a range of colors.

Time-resolved emission spectra (TRES) were acquired using a pulsed spectrofluorometer described in detail [27]. The laser system PL2251-20 with an Nd:YAG laser and a PG 401/SH optical parametric generator emitting pulses of FWHMz30 ps from EXSPLA was used as the excitation light source. The emission signal was analyzed by a Bruker Optics 2501S spectrograph and the Hamamatsu streak camera C4334-01 model. All operations were fully automated and controlled by the original Hamamatsu HPDTA software, which allows for real-time data analysis. By slicing the streak camera image at a certain time interval, the time decays were obtained.

### 3. Results and Discussion

#### 3.1. DSC Analysis

To analyze the thermal properties and the thermal stability of the prepared glasses, DSC measurements were performed. The results are presented in Figure 1. One can observe that the glass transition temperature depended on the SrF<sub>2</sub> content.  $T_g$  was located around 424 °C, 456 °C, and 459 °C for BBO, BBO+10SrF<sub>2</sub>, and BBO+20SrF<sub>2</sub> glasses, respectively. Interestingly, the exothermic maximum associated with crystallization was only visible for the BBO sample. The onset of crystallization peak temperature ( $T_x$ ) was located at 534 °C, which is well below the crystallization temperatures of the possible crystalline phases [11]. The glass stability region  $\Delta T$ , defined as the difference between  $T_x$  and  $T_g$ , for BBO glass was equal to 110 °C. This is a wide range, but even a small quantity of B<sub>2</sub>O<sub>3</sub> may have a positive effect on the thermal stability of this glass [29]. Taking into account the crystallization of the glasses, the thermal stability S parameter describing the glass resistance against devitrification was also determined [30]:

$$S = \frac{(T_c - T_x)(T_c - T_g)}{T_g} \quad (1)$$

In studied BBO glass, the calculated value of S is 8.72. For comparison, the values of S found in the literature for other borate glasses was even about 1 (50B<sub>2</sub>O<sub>3</sub>-50Bi<sub>2</sub>O<sub>3</sub> [31], 50Li<sub>2</sub>O-50B<sub>2</sub>O [32]). Unfortunately, such a significant difference between these values and the value obtained for our glass was not clear to us. As can be seen, the addition of SrF<sub>2</sub> to the base BBO composition led to the disappearance of the crystallization peak. Therefore, it can be said that it prevented the crystallization of the matrix. Unfortunately, no effect related to the crystallization of the SrF<sub>2</sub> phase in the BBO matrix was observed in these glasses.

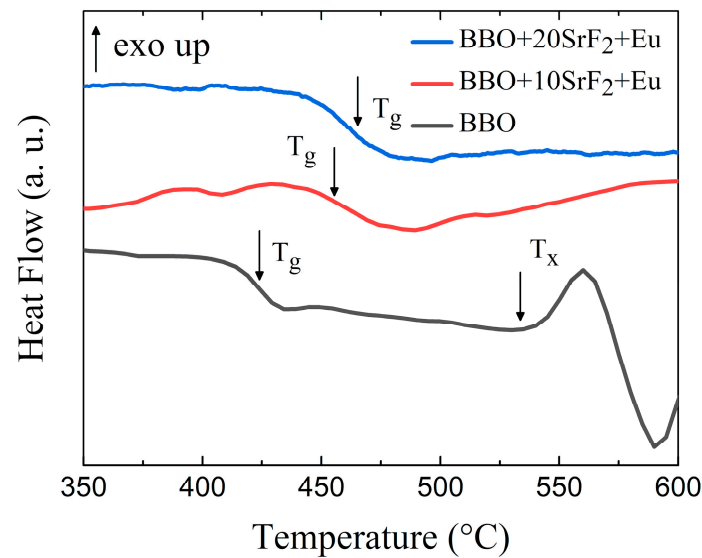


**Figure 1.** DSC curves of BBO, BBO+10SrF<sub>2</sub>, and BBO+20SrF<sub>2</sub> glasses.

### 3.2. XRD Analysis

The amorphous character of as-prepared glasses was confirmed by XRD studies. Figure 2 shows the diffraction patterns of BBO, BBO+10SrF<sub>2</sub>, and BBO+20SrF<sub>2</sub> glass samples. Only broad halos associated with amorphous materials can be seen.

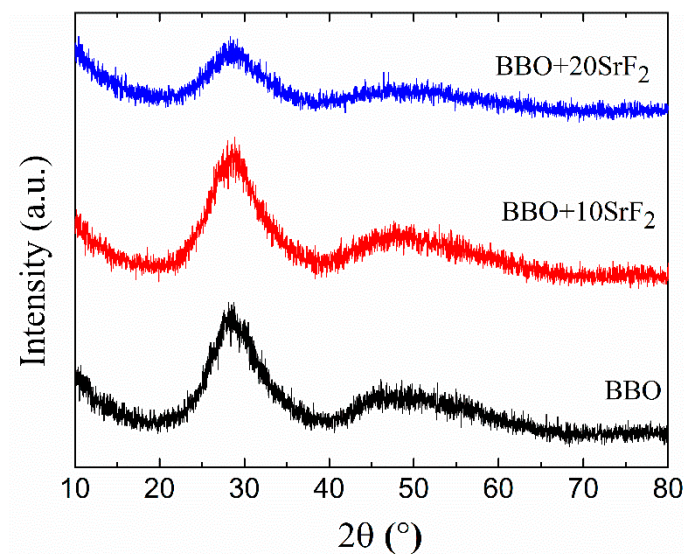


**Figure 2.** XRD patterns of as-prepared BBO, BBO+10SrF<sub>2</sub>, and BBO+20SrF<sub>2</sub> glasses.

The effect of the annealing temperature on the structure of the BBO+10SrF<sub>2</sub> and BBO+20SrF<sub>2</sub> glasses is shown in Figures 3 and 4. In Figure 3, X-ray diffractograms for the BBO+10SrF<sub>2</sub> and BBO+20SrF<sub>2</sub> glasses annealed at temperatures ranging from 560 to 590 °C for 1 h are presented. Figure 4 presents XRD patterns of these glasses after heat treatment in the same temperature range, but for 24 h. The aim of the thermal treatment was the growth of SrF<sub>2</sub> nanocrystals in the glass matrix. XRD patterns of the samples annealed at 560 °C did not differ from the patterns of the unannealed samples and showed a lack of long-range order. It should be noted, however, that in the presented XRD results a small amount of the nano-sized crystalline phase could have gone unnoticed, especially since the amorphous phase in which the nanocrystals were dispersed gives a broad halo in the range of 25–35 (2θ), in which there may be major reflections derived from the crystalline phases. Clear differences between BBO+10SrF<sub>2</sub> and BBO+20SrF<sub>2</sub> samples appeared after

annealing at 570 °C. XRD patterns of the BBO+10SrF<sub>2</sub> sample showed crystallization mainly in the BiBO<sub>3</sub> phase (Ref.Code 96-720-9482), but there were also visible low-intensity reflections corresponding to the SrF<sub>2</sub> phase (Ref.Code 96-900-9044). Unfortunately, there were also unidentified peaks in the diffractograms that were likely related to bismuth oxides, but crystalline borates sometimes have highly unusual stoichiometries [8]; therefore, it is difficult to fully characterize the presented diffraction pattern. On the other hand, BBO+20SrF<sub>2</sub> samples showed only the peaks characteristic of the SrF<sub>2</sub> crystalline phase (Ref.Code 96-900-9044). As can be seen, with the increase in the annealing temperature, the amount of BiBO<sub>3</sub> crystalline phase in the BBO+10SrF<sub>2</sub> samples decreased, whereas a weak reflection of the SrF<sub>2</sub> phase was already present in the sample annealed at 580 °C. In the case of the annealed BBO+20SrF<sub>2</sub> glass, the SrF<sub>2</sub> phase crystallized regardless of the temperature increase. The obtained diffractograms confirm the conclusion drawn based on DSC studies that the presence of SrF<sub>2</sub> in the BBO matrix prevented its crystallization. Unfortunately, annealing the samples at temperatures of 570 °C and higher caused them to begin to lose their transparency. Therefore, 560 °C was chosen as the temperature, providing a compromise between the transparency of the sample and the presence of a crystalline phase in it. At this temperature, only samples heated for 24 h became opaque.

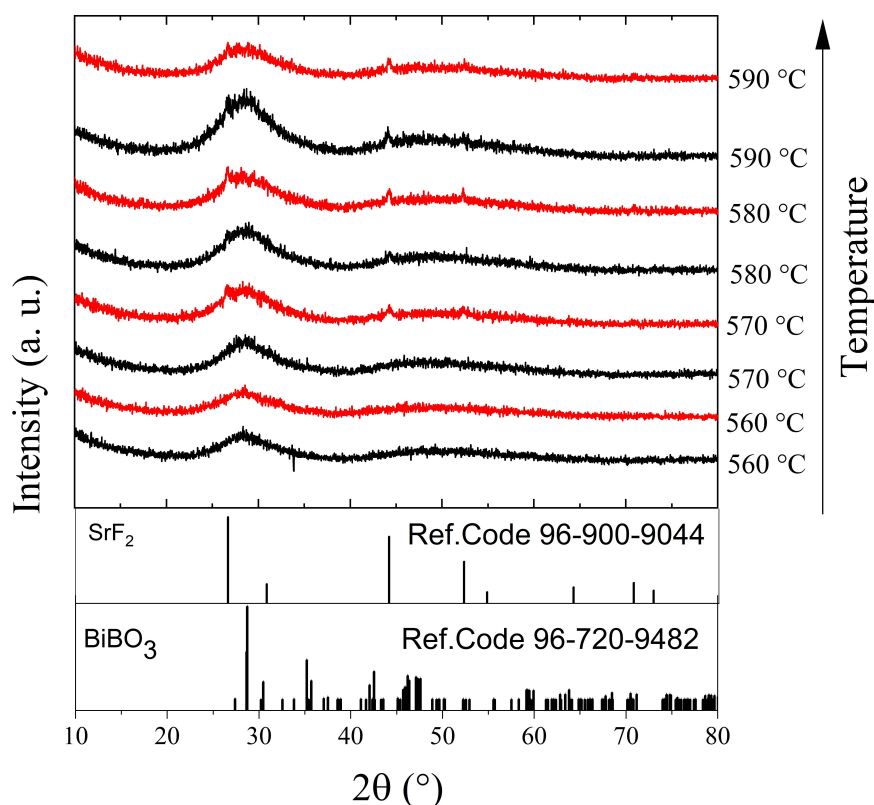


**Figure 3.** XRD patterns of BBO+10SrF<sub>2</sub> (black) and BBO+20SrF<sub>2</sub> (red) glasses after annealing in the temperature range of 560–590 °C for 1 h.

### 3.3. FTIR Analysis

Changes in the structure of the studied glasses occurring due to annealing were also visible in the FTIR spectra. The FTIR spectra obtained for BBO+10SrF<sub>2</sub> and BBO+20SrF<sub>2</sub> glasses and glass-ceramics are shown in Figure 5a,b, respectively. For comparison, the spectrum of as-prepared BBO glass was added to each figure. It is well known that the network of borate glasses is mainly constructed from [BO<sub>3</sub>] triangular structural units, which under the influence of the modifier can transform into [BO<sub>4</sub>] tetrahedral units. Such a change can also occur under the influence of Bi<sub>2</sub>O<sub>3</sub> [12]. The broad absorption bands in the region of 680–720 cm<sup>-1</sup> and 1100–1250 cm<sup>-1</sup> are usually assigned to deformation and stretching

vibrations of  $[\text{BO}_3]$  groups [10,13,33]. In addition, the band at about  $1200\text{--}1400\text{ cm}^{-1}$  can be attributed to the stretching vibration of  $[\text{BO}_3]$ . On the other hand, the presence of  $[\text{BO}_4]$  groups may be indicated by the band at  $900\text{--}1100\text{ cm}^{-1}$  [13,33]. However, it should be noted that these bands may shift under the influence of  $\text{Bi}_2\text{O}_3$  and overlap with the  $\text{Bi}_2\text{O}_3$  peaks and shoulders [33]. Looking at the spectra presented in Figure 5, it can be concluded that the annealing did not significantly affect them.

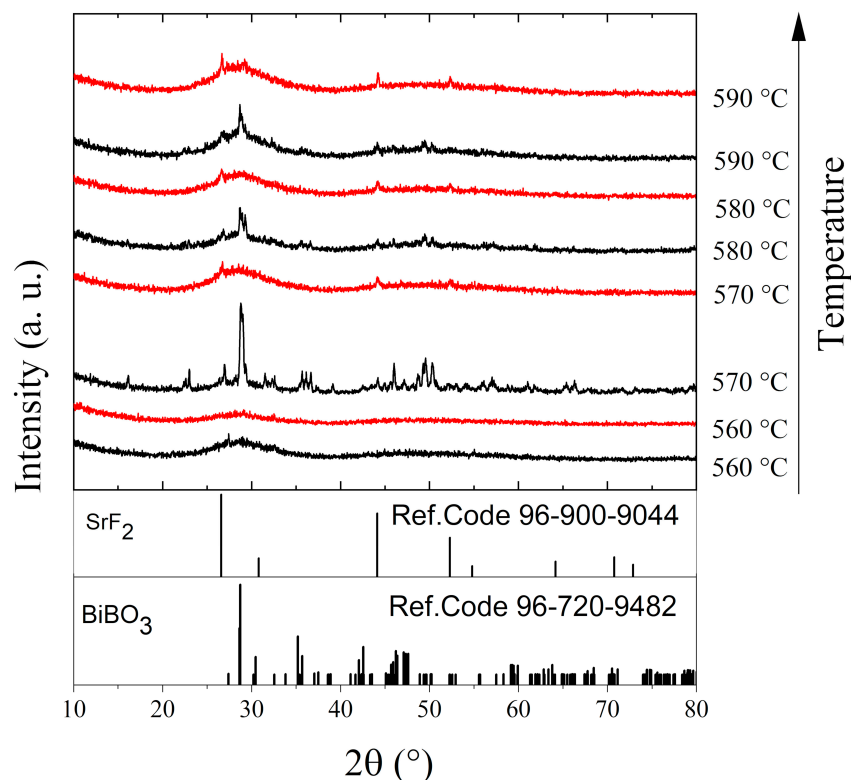


**Figure 4.** XRD patterns of  $\text{BBO}+10\text{SrF}_2$  (black) and  $\text{BBO}+20\text{SrF}_2$  (red) glasses after annealing in the temperature range of  $560\text{--}590\text{ }^\circ\text{C}$  for 24 h.

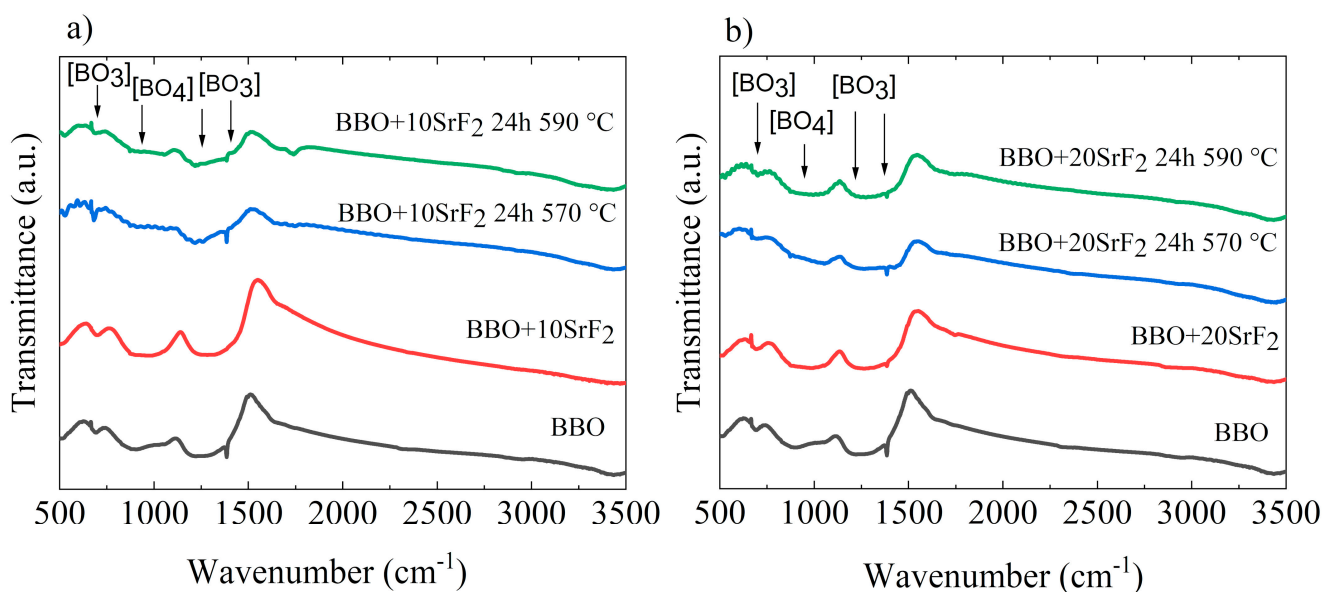


**Figure 5.** FTIR spectra of  $\text{BBO}+10\text{SrF}_2$  (a) and  $\text{BBO}+20\text{SrF}_2$  (b) as-prepared glasses and glasses after annealing at  $570\text{ }^\circ\text{C}$  and  $590\text{ }^\circ\text{C}$ . For comparison, the spectrum of as-prepared BBO glass was added to each figure.

### 3.4. XPS Analysis

XPS analysis was performed to provide additional information about the valence states of the elements of which the samples consisted. Particular emphasis was placed on the study of the valence states of Eu and Bi ions, as well as the chemical states of Sr that could indicate Sr chemical bonds with both fluorine and oxygen [24,34,35]. As research has shown, both Eu and Bi ions are in the 3+ valence state. Exemplary spectra of the Sr region of BBO+10SrF<sub>2</sub> and BBO+20SrF<sub>2</sub> glasses and glass ceramics after annealing at 560 °C for 24 h are shown in Figure 6. All spectra consisted of the Sr 3d spin-orbit doublet, but a detailed analysis of these peaks suggests the presence of more than one chemical state of Sr in all samples. Peaks at 133.5 and 135.5 eV could be assigned to the Sr 3d<sub>5/2</sub> and Sr 3d<sub>3/2</sub> in Sr-O [34,35], whereas peaks with energies equal to 134.0 and 136.0 eV could be attributed to Sr 3d<sub>5/2</sub> and Sr 3d<sub>3/2</sub> in Sr-F [34,35]. The contribution of Sr-O and Sr-F doublets in the glasses was 59% and 41% (BBO+10SrF<sub>2</sub>) and 67% and 33% (BBO+20SrF<sub>2</sub>), respectively. The contribution of Sr-O and Sr-F doublets after annealing was, respectively, 80% and 20% (BBO+10SrF<sub>2</sub>) and 52% and 48% (BBO+20SrF<sub>2</sub>). Therefore, as can be seen, annealing did not change the ratio of the doublets in the same way in both samples. The increase in the contribution of the Sr-F doublet, which in turn indicated an increase in the amount of the SrF<sub>2</sub> crystal phase in the matrix, only took place in samples containing 20 mol % SrF<sub>2</sub>. However, as the analysis of the X-ray diffractograms showed, SrF<sub>2</sub> as the only crystalline phase was also present only in the samples containing 20 mol % SrF<sub>2</sub>. Therefore, it can be concluded from both of these methods that the formation of SrF<sub>2</sub> nanocrystals hindered the crystallization of the matrix.

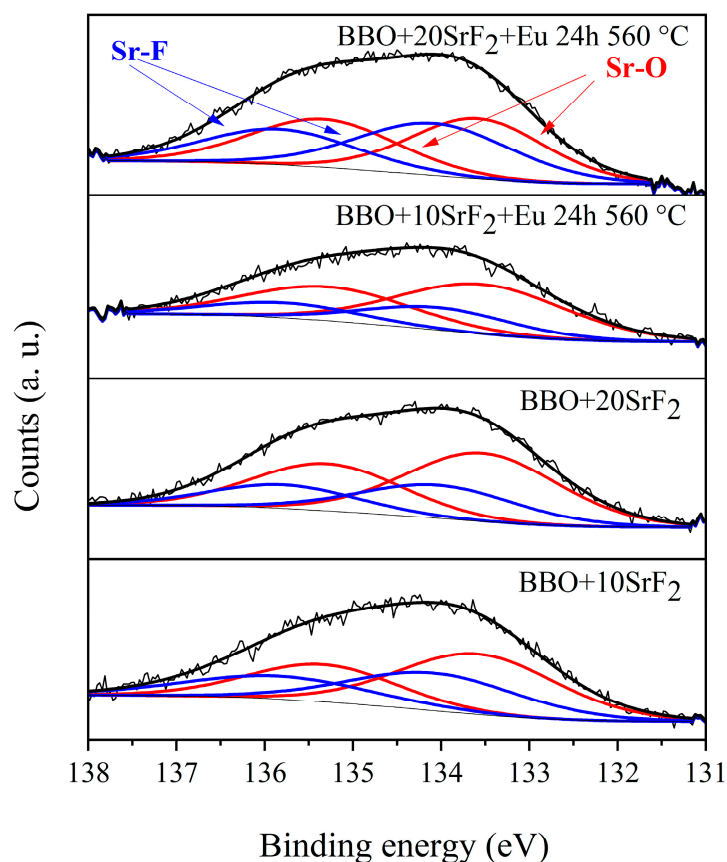


**Figure 6.** Sr 3D region of XPS spectra of BBO+10SrF<sub>2</sub> and BBO+20SrF<sub>2</sub> as-prepared glasses and glasses after annealing at 560 °C for 24 h.

### 3.5. Luminescence Analysis

Luminescence properties of Eu-doped BBO, BBO+10SrF<sub>2</sub>, and BBO+20SrF<sub>2</sub> glasses and glass-ceramics were investigated to determine the influence of SrF<sub>2</sub> on the luminescence intensity of Eu<sup>3+</sup> ions. Figures 7a and 8a show the excitation spectra of as-prepared BBO+10SrF<sub>2</sub>+Eu and BBO+20SrF<sub>2</sub>+Eu glasses monitored at the wavelength of  $\lambda_{em} = 615$  nm, which corresponds to <sup>5</sup>D<sub>0</sub> → <sup>7</sup>F<sub>2</sub> transition of Eu<sup>3+</sup> ions [3,36]. Several characteristics for 4f-4f transition peaks were visible in the spectrum. Excitation bands at 382 and 465 nm may have been assigned to <sup>7</sup>F<sub>0</sub> → <sup>5</sup>G<sub>4</sub>, <sup>5</sup>D<sub>2</sub> transitions, whereas bands at 396, 415, and 533 nm originated from <sup>7</sup>F<sub>0</sub> → <sup>5</sup>L<sub>6</sub>, <sup>5</sup>D<sub>3</sub>, and <sup>5</sup>D<sub>1</sub> transitions, respectively [3,36]. A wavelength of 465 nm was selected for the observation of the emission spectra. This is the line with the highest intensity in the excitation spectrum. Emission spectra of BBO+10SrF<sub>2</sub>+Eu glass and glass-ceramics crystallized at 560 °C (Figure 7b) consisted of several bands corresponding to Eu<sup>3+</sup> radiative transitions at 581 nm (<sup>5</sup>D<sub>0</sub> → <sup>7</sup>F<sub>0</sub>), 594 nm (<sup>5</sup>D<sub>0</sub> → <sup>7</sup>F<sub>1</sub>), 615 nm (<sup>5</sup>D<sub>0</sub> → <sup>7</sup>F<sub>2</sub>), 655 nm (<sup>5</sup>D<sub>0</sub> → <sup>7</sup>F<sub>3</sub>), and 703 nm (<sup>5</sup>D<sub>0</sub> → <sup>7</sup>F<sub>4</sub>) [3,36]. As can be seen, there were no significant differences between the intensity of the bands corresponding to the BBO+Eu glass and the glass with the addition of 10 mol % of SrF<sub>2</sub>. In addition, annealing of the BBO+10SrF<sub>2</sub>+Eu samples did not change the intensity of the spectral lines. However, if we look at the results concerning the structure of the annealed samples, the crystallization of the borane-bismuth matrix, apart from the SrF<sub>2</sub> crystal phase, cannot be ruled out. Assuming that this is the case, the emitted radiation could undergo scattering on defects. Looking at the emission spectra corresponding to the BBO+20SrF<sub>2</sub>+Eu samples (Figure 8b), it can be noticed that the emission bands were at the same wavelengths as for the samples with 10 mol % of SrF<sub>2</sub>. In addition, it is evident that annealing affected the intensity of Eu<sup>3+</sup> ions emission. It is worth noticing that the SrF<sub>2</sub> crystalline phase was characterized by considerably lower phonon energy compared to the oxide materials. Therefore, if Eu<sup>3+</sup> ions are located in the SrF<sub>2</sub> nanocrystals, this leads to a decrease in multi-phonon relaxation probability, and consequently to an increase in emission efficiency. This was also the case with other strontium fluoride-containing glass ceramics [25,37].

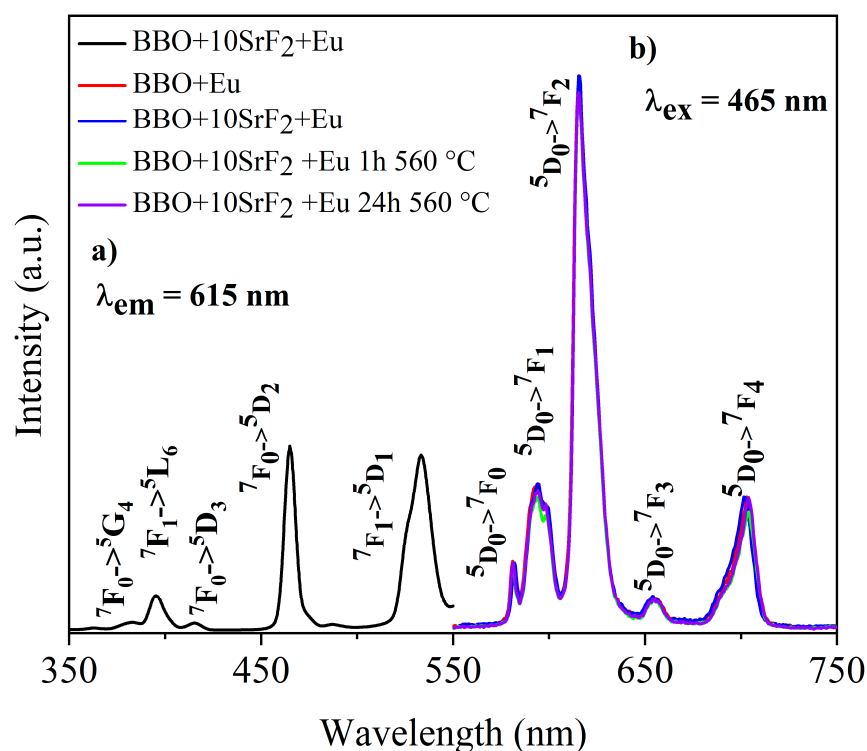


**Figure 7.** The excitation spectrum of BBO+10SrF<sub>2</sub>+Eu glass (a), and the emission spectra of BBO+Eu glass, and BBO+10SrF<sub>2</sub>+Eu glass and glass-ceramics after annealing at 560 °C for 1 h and 24 h (b).



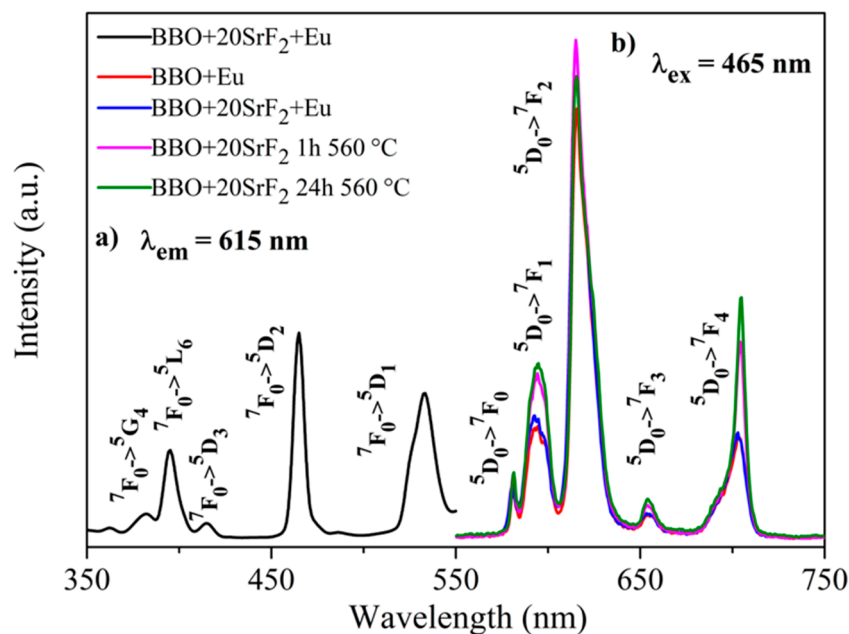


**Figure 8.** The excitation spectrum of BBO+20SrF<sub>2</sub>+Eu glass (a), and the emission spectra of BBO+Eu glass, and BBO+20SrF<sub>2</sub>+Eu glass and glass-ceramics after annealing at 560 °C for 1 h and 24 h (b).

### 3.6. Luminescence Decay and Judd–Ofelt Analysis

Luminescence decay analysis was performed on as-prepared Eu doped BBO, BBO+10SrF<sub>2</sub> and BBO+20SrF<sub>2</sub> glasses and glass-ceramics. The decay curves were obtained by monitoring <sup>5</sup>D<sub>0</sub> → <sup>7</sup>F<sub>2</sub> emission line (λ<sub>em</sub> = 615 nm) upon excitation at λ<sub>exc</sub> = 465 nm (<sup>7</sup>F<sub>0</sub> → <sup>5</sup>D<sub>2</sub> transition) and are shown in Figure 9a,b.

It was found that luminescence decays in both cases can be described as two-exponential decays according to the following equation [38]:

$$I(t) = A_1 \exp\left(\frac{-t}{\tau_1}\right) + A_2 \exp\left(\frac{-t}{\tau_2}\right) \quad (2)$$

where τ<sub>1</sub> and τ<sub>2</sub> are long and short luminescence lifetime components contributing to the average lifetime (τ<sub>avg</sub>), and A<sub>1</sub> and A<sub>2</sub> are amplitudes of respective decay components. The lifetimes τ<sub>1</sub> and τ<sub>2</sub>, amplitudes, and average lifetime calculated for the luminescence decay curves presented in Figure 9 are collected in Table 1.

**Table 1.** Fitting parameters of the luminescence decays, calculated Judd–Ofelt parameters, and luminescence intensity ratios.

	BBO+Eu	BBO+10SrF <sub>2</sub> +E	BBO+20SrF <sub>2</sub> +Eu	BBO+10SrF <sub>2</sub> +Eu 1 h 560 °C	BBO+10SrF <sub>2</sub> +Eu 24 h 560 °C	BBO+20SrF <sub>2</sub> +Eu 1 h 560 °C	BBO+20SrF <sub>2</sub> +Eu 24 h 560 °C
A <sub>1</sub>	3913	4148	4267	3297	3431	3440	3338
A <sub>2</sub>	3237	3115	2951	3893	3387	3046	2692
τ <sub>1</sub> (ms)	1.2	1.18	1.28	1.24	1.22	1.45	1.48
τ <sub>2</sub> (ms)	0.56	0.5	0.52	0.58	0.56	0.66	0.65
<τ <sub>avg</sub> > (ms)	1	1	1.1	1	1	1.2	1.2
Ω <sub>2</sub>	5.64	5.15	5.54	6.06	5.86	4.48	5.11
Ω <sub>4</sub>	3.89	3.74	3.59	3.78	3.85	3.86	4.07
R/O	3.76	3.45	3.69	4.04	3.90	3.06	2.73

This double-exponential nature of the decay curves indicates the presence of two different surroundings of Eu<sup>3+</sup> ions. Long lifetime (τ<sub>1</sub>) is correlated with higher symmetry of the crystal field, whereas short lifetime (τ<sub>2</sub>) is associated with lower symmetry of the Eu<sup>3+</sup> surroundings. Thus, in glasses containing SrF<sub>2</sub> or PbF<sub>2</sub> nanocrystals, a long

lifetime is attributed to  $\text{Eu}^{3+}$  ions, which are located in the nanocrystals, and short lifetimes correspond to the ions incorporated into the amorphous matrix [24,25,37,39].

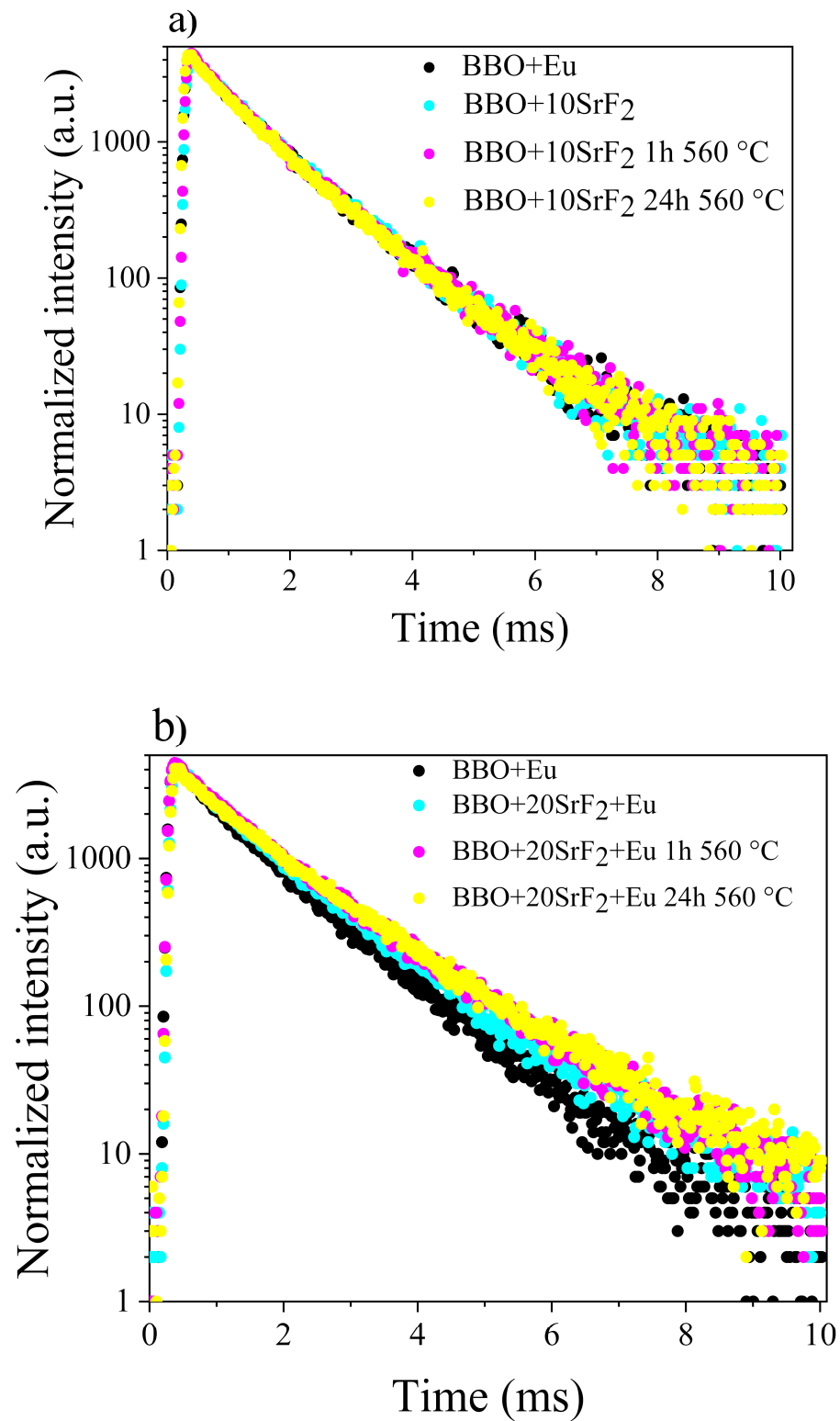


**Figure 9.** Luminescence decay curves of Eu-doped BBO and BBO+10SrF<sub>2</sub> samples (a) Eu-doped BBO and BBO+20SrF<sub>2</sub> samples (b).

Concerning the tested samples, it can therefore be said that  $\tau_1$  represents the lifetime of  $\text{Eu}^{3+}$  ions incorporated into the SrF<sub>2</sub> nanocrystals, whereas  $\tau_2$  corresponded to ions

surrounded by the glass matrix. However, in the case of the studied samples, the situation seems to be more complicated. Two lifetimes were also observed in BBO+Eu glass, which did not contain strontium fluoride, and if to compare the results obtained for this glass with the values calculated for the BBO+10SrF<sub>2</sub> sample, the lifetimes are not much different. This means that the tested glass may have contained nanocrystalline areas that were formed during the glass preparation process, which are not visible in diffraction studies. Especially in borate glasses with various dopants, single exponential decay curves are usually observed [40,41]. As can be seen, the longest  $\tau_2$  lifetime was observed for the BBO+20SrF<sub>2</sub> samples, especially those annealed for 24 h at 560 °C. It seems that in these samples the amount of Eu<sup>3+</sup> ions incorporated into SrF<sub>2</sub> nanocrystals increased. This result is in line with the results obtained with the XRD. They show that SrF<sub>2</sub> as the only crystalline phase in the glass was present at 20 mol% of SrF<sub>2</sub>, whereas at 10 mol% the matrix crystallization also took place.

Changes in symmetry in the surroundings of the europium ions, as well as changes in the degree of covalence of bonds of these ions, can be observed based on Judd–Ofelt parameters. The Judd–Ofelt parameters  $\Omega_2$  and  $\Omega_4$  were calculated based on luminescence emission spectra using JOES application software and are presented in Table 1. Detailed information regarding software and calculations can be found in reference [42]. The  $\Omega_6$  parameter was not determined in this study due to the unregistered emission band, located in the NIR range of wavelength, that corresponds to the  $^5D_0 \rightarrow ^7F_6$  transition band. The  $\Omega_2$  parameter is known to be structure sensitive and also depends on the covalence of Eu<sup>3+</sup> bonds with the ligand [43–46]. It is determined from  $^5D_0 \rightarrow ^7F_2$  hypersensitive transition. The high value of the  $\Omega_2$  parameter ( $\Omega_2 > \Omega_4$ ) suggests that Eu<sup>3+</sup> ions occupied mostly low-symmetry sites. This corresponds to the situation where Eu<sup>3+</sup> ions were mainly located in the glassy matrix. On the other hand, the Eu–O bond in the glasses was highly covalent, which was also reflected in the high  $\Omega_2$  coefficients. In turn, the  $\Omega_4$  parameter is related to the rigidity of glasses and is often attributed to the emergence of long-range effects related to crystal lattice [19]. Therefore, the processes of crystallization of glasses should consequently lead to an increase in this parameter. This behavior was observed, for example, in tellurite glass-ceramics containing SrF<sub>2</sub> nanocrystals [25]. The parameters  $\Omega_2$  and  $\Omega_4$  calculated for the BBO+10SrF<sub>2</sub> and BBO+20SrF<sub>2</sub> glasses before and after annealing were different, but the change due to crystallization depended on the initial amount of SrF<sub>2</sub>. In the BBO+10SrF<sub>2</sub> sample, both  $\Omega_2$  and  $\Omega_4$  were higher in the annealed samples. Nevertheless, it is a sample where it was difficult to say that SrF<sub>2</sub> was the only crystalline phase in the glass matrix and it was, therefore, difficult to analyze the influence of the appearance of SrF<sub>2</sub> nanocrystals on luminescence. On the other hand, in the case of the BBO+20SrF<sub>2</sub> sample, after crystallization the parameter  $\Omega_2$  was lower and  $\Omega_4$  was higher than in as-prepared glass. However, in the BBO glass containing 20 mol% of SrF<sub>2</sub>, no additional crystallization of the matrix was observed after annealing; hence, it can be concluded that the observed change in the values of  $\Omega_2$  and  $\Omega_4$  parameters, as well as the increase in  $\tau_1$  time, are because Eu<sup>3+</sup> ions were located in SrF<sub>2</sub> nanocrystals.

These results follow the luminescence intensity ratio R (asymmetry ratio), which in the case of Eu<sup>3+</sup> ions can be calculated from the expression [45]:

$$R = \frac{I(^5D_0 \rightarrow ^7F_2)}{I(^5D_0 \rightarrow ^7F_1)} \quad (3)$$

The transition  $^5D_0 \rightarrow ^7F_1$  occurs via magnetic dipole and is independent of the host matrix, whereas  $^5D_0 \rightarrow ^7F_2$  has a pure electric dipole moment origin and is hypersensitive to changes in the crystal field around Eu<sup>3+</sup> ions. In other words, a more intense  $^5D_0 \rightarrow ^7F_2$  transition indicates that the Eu<sup>3+</sup> ions mainly occupy positions without an inversion center, whereas a more intense  $^5D_0 \rightarrow ^7F_1$  transition shows that the Eu<sup>3+</sup> ions are located at sites with higher symmetry. Therefore, with the change in site symmetry of Eu<sup>3+</sup> ions, when they take positions with higher symmetry, the asymmetry ratio coefficient should decrease. The intensity ratios calculated for the as-prepared BBO+20SrF<sub>2</sub> sample and

the samples after annealing at 560 °C decreased with an increase in the annealing time (resulting in the growth of SrF<sub>2</sub> nanocrystals). This means that some of the Eu<sup>3+</sup> ions were located in the structure of nanocrystals. Unfortunately, as shown earlier, BBO glass initially containing 10 mol % of SrF<sub>2</sub> may behave differently, which is most likely related to the not-completely-amorphous (after annealing) borate-bismuth matrix.

#### 4. Conclusions

In summary, borate-bismuth glass-ceramics doped with Eu<sup>3+</sup> ions, with SrF<sub>2</sub> nanocrystals, were obtained. The structural modifications of parental glass, leading to SrF<sub>2</sub> nanostructure crystallization, depend strongly on the initial amount of strontium fluoride. In the case of borate-bismuth glass, it is possible to obtain at least five stable crystalline phases of Bi<sub>2</sub>O<sub>3</sub>-B<sub>2</sub>O<sub>3</sub> [11], and 10 mol % of SrF<sub>2</sub> introduced into the glass is insufficient to block crystallization of the matrix. This has a strong influence on the luminescent properties. The expected increase in the intensity of emission bands was not observed in such glass ceramics, which was probably related to the scattering of the emitted radiation on various types of defects occurring during the annealing of the glasses. The increase in luminescence intensity was observed after annealing in samples containing 20 mol% SrF<sub>2</sub>. The luminescence lifetimes obtained for these glass-ceramics indicate that some of the Eu<sup>3+</sup> ions were located in SrF<sub>2</sub> nanocrystals. This was also confirmed by the analysis of the Judd–Ofelt parameters  $\Omega_2$  and  $\Omega_4$ , and luminescence intensity ratio R. It can therefore be concluded that the glasses and glass-ceramics described in this work could be considered as potential candidates for LED phosphors.

**Author Contributions:** Conceptualization, B.K. and K.M.; methodology, K.M., M.M., A.S.; M.L., A.M.-G., W.S., and B.K.; formal analysis, K.M. and B.K.; investigation, K.M. and B.K.; data curation, K.M. and B.K.; writing—original draft preparation, B.K. and K.M.; writing—review and editing, K.M., M.M., A.S., M.L., W.S., and B.K.; supervision, B.K. All authors have read and agreed to the published version of the manuscript.

**Funding:** This research received no external funding.

**Data Availability Statement:** The data presented in this study (FTIR and luminescence) are openly available at: <https://mostwiedzy.pl/pl/open-research-data/luminescence-and-ftir-measurements-of-b2o3-bi2o3-srf2-glass-and-glass-ceramics-doped-with-eu3-ions,629025230630285-0> (accessed on 30 June 2020).

**Acknowledgments:** The authors would like to thank Leon Murawski for the fruitful discussions.

**Conflicts of Interest:** The authors declare no conflict of interest.

#### References

1. El-Mallawany, R. *Tellurite Glass Smart Materials, Applications in Optics and Beyond*; Springer International Publishing AG, Part of Springer Nature: Cham, Switzerland, 2018; ISBN 978-3-319-76567-9. [CrossRef]
2. Nagaraja Naick, B.; Damodaraiah, S.; Reddy Prasad, V.; Vijaya Lakshmi, R.P.; Ratnakaram, Y.C. Judd-Ofelt analysis and luminescence studies on Dy<sup>3+</sup>-doped different phosphate glasses for white light emitting material applications. *Opt. Int. J. Light Electron Opt.* **2019**, *192*, 162980. [CrossRef]
3. Zhao, C.; Cai, J.; Li, R.; Tie, S.; Wan, X.; Shen, J. White light emission from Eu<sup>3+</sup>/Tb<sup>3+</sup>/Tm<sup>3+</sup> triply-doped aluminoborate glass excited by UV light. *J. Non-Cryst. Solids* **2012**, *358*, 604–608. [CrossRef]
4. Gonçalves, M.C.; Santos, L.F.; Almeida, R.M. Rare-earth-doped transparent glass ceramics. *C. R. Chim.* **2002**, *5*, 845–854. [CrossRef]
5. Dumbaugh, W.H.; Lapp, J.C. Heavy-metal oxide glasses. *J. Am. Ceram. Soc.* **1992**, *75*, 2315–2326. [CrossRef]
6. Fan, H.; Gao, G.; Wang, G.; Hu, J.; Hu, L. Tm<sup>3+</sup> doped Bi<sub>2</sub>O<sub>3</sub>-GeO<sub>2</sub>-Na<sub>2</sub>O glasses for 1.8 μm fluorescence. *Opt. Mater.* **2010**, *32*, 627–631. [CrossRef]
7. Majerus, O.; Trégouët, H.; Caurant, D.; Pytalev, D. Comparative study of the rare earth environment in rare earth metaborate glass (REB<sub>3</sub>O<sub>6</sub>, RE = La, Nd) and in sodium borate glasses. *J. Non-Cryst. Solids* **2015**, *425*, 91–102. [CrossRef]
8. Wright, A.C. My Borate Life: An Enigmatic Journey. *Int. J. Appl. Glass Sci.* **2015**, *6*, 45–63. [CrossRef]
9. Wright, A.C. Borate structures: Crystalline and vitreous. *Phys. Chem. Glasses* **2010**, *51*, 1–39.
10. Bobkova, N.M. Properties and Structure of Bismuth-Borate Glasses. *Glass Ceram.* **2016**, *72*, 360–365. [CrossRef]
11. Bajaj, A.; Khanna, A. Crystallization of bismuth borate glasses. *J. Phys. Condens. Matter* **2009**, *21*, 035112. [CrossRef] [PubMed]

12. Bobkova, N.M. Characteristic of the Structure State of Bismuth Ions in Bismuth-Borate Glasses. *Glass Ceram.* **2019**, *75*, 383–386. [[CrossRef](#)]
13. Pascuta, P.; Pop, L.; Rada, S.; Bosca, M.; Culea, E. The local structure of bismuth borate glasses doped with europium ions evidenced by FTIR spectroscopy. *J. Mater. Sci. Mater. Electron.* **2008**, *19*, 424–428. [[CrossRef](#)]
14. Pisarski, W.A.; Pisarska, J.; Maczka, M.; Lisiecki, R.; Grobelny, Ł.; Goryczka, T.; Dominiak-Dzik, G.; Ryba-Romanowski, W. Rare earth-doped lead borate glasses and transparent glass-ceramics: Structure-property relationship. *Spectrochim. Acta Part A* **2011**, *27*, 696–700. [[CrossRef](#)] [[PubMed](#)]
15. Pisarski, W.A.; Pisarska, J.; Ryba-Romanowski, W. Structural role of rare earth ions in lead borate glasses evidenced by infrared spectroscopy:  $\text{BO}_3 \leftrightarrow \text{BO}_4$  conversion. *J. Mol. Struct.* **2005**, *744*, 515–520. [[CrossRef](#)]
16. Hopper, R.W. Stochastic theory of scattering from idealized spinodal structures: II. Scattering in general and for the basic late stage model. *J. Non-Cryst. Solids* **1985**, *70*, 111–142. [[CrossRef](#)]
17. Mattarelli, M.; Tikhomirov, V.K.; Seddon, A.B.; Montagna, M.; Moserm, E.; Chiasera, A.; Chaussedent, S.; Conti, G.N.; Pelli, G.L.; Righini, C.; et al.  $\text{Tm}^{3+}$ -activated transparent oxy-fluoride glass-ceramics: Structural and spectroscopic properties. *J. Non-Cryst. Solids* **2004**, *346*, 354–358. [[CrossRef](#)]
18. Boulard, B.; Péron, O.; Jestin, Y.; Ferrari, M.; Duverger-Arfuso, C. Characterization of  $\text{Er}^{3+}$ -doped fluoride glass ceramics waveguides containing  $\text{LaF}_3$  nanocrystals. *J. Lumin.* **2009**, *129*, 1637–1640. [[CrossRef](#)]
19. Rodríguez, V.D.; Lavín, V.; Rodríguez-Mendoza, U.R.; Martín, I.R. Spectroscopy of rare earth ions of fluoride glasses for laser applications. *Opt. Mater.* **1990**, *13*, 1–7. [[CrossRef](#)]
20. Gao, Y.; Hu, Y.; Zhou, D.; Qiu, J. Effect of heat treatment mechanism on upconversion luminescence in  $\text{Er}^{3+}/\text{Yb}^{3+}$  co-doped  $\text{NaYF}_4$  oxyfluoride glass-ceramics. *J. Alloys. Compd.* **2017**, *699*, 303–307. [[CrossRef](#)]
21. Bae, S.R.; Choi, Y.G.; Bin, W.I.; Lee, K.S.; Chung, W.J. Rare earth doped silicate-oxyfluoride glass ceramics incorporating  $\text{LaF}_3$  nano-crystals for UV-LED color conversion. *Opt. Mater.* **2013**, *35*, 2034–2038. [[CrossRef](#)]
22. Zur, L.; Thi, L.; Tran, N.; Meneghetti, M.; Thanh, V.T.; Righini, G.C. Tin-dioxide nanocrystals as  $\text{Er}^{3+}$  luminescence sensitizers: Formation of glass-ceramic thin films and their characterization. *Opt. Mater.* **2017**, *63*, 95–100. [[CrossRef](#)]
23. Chen, D.; Xiang, W.; Liang, X.; Zhong, J.; Yu, H.; Ding, M.; Lu, H.; Ji, Z. Advances in transparent glass-ceramic phosphors for white light-emitting diodes—A review. *J. Eur. Ceram. Soc.* **2015**, *35*, 859–869. [[CrossRef](#)]
24. Walas, M.; Lewandowski, T.; Synak, A.; Łapiński, M.; Sadowski, W.; Kościelska, B.  $\text{Eu}^{3+}$  doped tellurite glass ceramics containing  $\text{SrF}_2$  nanocrystals: Preparation, structure and luminescence properties. *J. Alloys Compd.* **2017**, *696*, 619–626. [[CrossRef](#)]
25. Walas, M.; Lisowska, M.; Lewandowski, T.; Becerro, A.I.; Łapiński, M.; Synak, A.; Sadowski, W.; Kościelska, B. From structure to luminescence investigation of oxyfluoride transparent glasses and glass-ceramics doped with  $\text{Eu}^{3+}/\text{Dy}^{3+}$  ions. *J. Alloys Compd.* **2019**, *806*, 1410–1418. [[CrossRef](#)]
26. Miguel, A.; Morea, R.; Arriandiaga, M.A.; Hernandez, M.; Ferrer, F.J.; Domingo, C.; Fernandez-Navarro, J.M.; Gonzalo, J.; Fernandez, J.; Balda, R. Structural, optical, and spectroscopic properties of  $\text{Er}^{3+}$ -doped  $\text{TeO}_2\text{-ZnO-ZnF}_2$  glass-ceramics. *J. Eur. Ceram. Soc.* **2014**, *34*, 3959–3968. [[CrossRef](#)]
27. Grobelna, B.; Bojarski, P.; Kuklinski, B.; Kubicki, A.A.; Synak, A. Optical properties and luminescence kinetics of  $\text{Ln}_{1.9}\text{Pr}_{0.1}(\text{WO}_4)_3$  (where Ln = Gd, La) immobilized in silica xerogel. *Opt. Mater.* **2011**, *34*, 103–108. [[CrossRef](#)]
28. Becker, P.; Fröhlich, R.Z. Crystal Growth and Crystal Structure of the Metastable Bismuth Orthoborate  $\text{BiBO}_3$ . *Naturforsch* **2004**, *59b*, 256–258. [[CrossRef](#)]
29. Yanmin, Y.; Yanzhou, L.; Peiqing, C.; Maalej, R.; Seo, H.J. Thermal stability and spectroscopic properties of  $\text{Ho}^{3+}$  doped tellurite-borate glasses. *J. Rare Earths* **2015**, *33*, 939–945. [[CrossRef](#)]
30. Saad, M.; Poulain, M. Glass Forming Ability Criterion. *Mater. Sci. Forum.* **1987**, *19–20*, 1–18. [[CrossRef](#)]
31. Ferreira, E.B.; Zanutto, E.D.; Feller, S.; Lodden, G.; Banerjee, J.; Edwards, T.; Affatigato, M. Critical Analysis of Glass Stability Parameters and Application to Lithium Borate Glasses. *J. Am. Ceram. Soc.* **2011**, *94*, 3833–3841. [[CrossRef](#)]
32. Mary, N.; Rebours, M.; Castel, E.; Vaishnav, S.; Deng, W.; Bell, A.M.; Clegg, F.; Allsopp, B.L.; Scrimshire, A.; Bingham, P.A. Enhanced thermal stability of high-bismuth borate glasses by addition of iron. *J. Non-Cryst. Solids* **2018**, *500*, 149–157. [[CrossRef](#)]
33. Ali, A.A.; Rammahb, Y.S.; El-Mallawany, R.; Souri, D. FTIR and UV spectra of pentateryary borate glasses. *Measurement* **2017**, *105*, 72–77. [[CrossRef](#)]
34. Yagoub, M.Y.A.; Swart, H.C.; Noto, L.L.; O’Connell, J.H.; Lee, M.E.; Coetsee, E. The effects of Eu-concentrations on the luminescent properties of  $\text{SrF}_2$ : Eu nanophosphor. *J. Lumin.* **2014**, *156*, 150–156. [[CrossRef](#)]
35. Yagoub, M.Y.A.; Swart, H.C.; Coetsee, E. Concentration quenching, surface and spectral analyses of  $\text{SrF}_2$ : $\text{Pr}^{3+}$  prepared by different synthesis techniques. *Opt. Mater.* **2015**, *42*, 204–209. [[CrossRef](#)]
36. Sontakke, A.D.; Tarafder, A.; Biswas, K.; Annapurna, K. Sensitized red luminescence from  $\text{Bi}^{3+}$  co-doped  $\text{Eu}^{3+}$ :  $\text{ZnO-B}_2\text{O}_3$  glasses. *Phys. B Condens. Matter* **2009**, *404*, 3525–3529. [[CrossRef](#)]
37. Luo, Q.; Qiao, X.; Fan, X.; Liu, S.; Yang, H.; Zhang, X. Reduction and luminescence of europium ions in glass ceramics containing  $\text{SrF}_2$  nanocrystals. *J. Non-Cryst. Solids* **2008**, *354*, 4691–4694. [[CrossRef](#)]
38. Yu, C.; Yang, X.; Huang, A.; Chai, Z.; Qiu, J.; Song, Z.; Zhou, D. Photoluminescence properties of tellurite glasses doped  $\text{Dy}^{3+}$  and  $\text{Eu}^{3+}$  for the UV and blue converted WLEDs. *J. Non-Cryst. Solids* **2017**, *457*, 1–8. [[CrossRef](#)]
39. Szpikowska-Sroka, B.; Pawlik, N.; Goryczka, T.; Pisarski, W.A. Effect of the initial reagents concentration on final crystals size and luminescence properties of  $\text{PbF}_2$ : $\text{Eu}^{3+}$  phosphors. *J. Alloys Compd.* **2008**, *730*, 150–160. [[CrossRef](#)]

40. Jamalaiah, B.C.; Suresh Kumar, J.; Mohan Babu, A.; Rama Moorthy, L. Spectroscopic studies of  $\text{Eu}^{3+}$  ions in LBTAf glasses. *J. Alloys Compd.* **2009**, *478*, 63–67. [[CrossRef](#)]
41. Venkatramu, V.; Babu, P.; Jayasankar, C.K. Fluorescence properties of  $\text{Eu}^{3+}$  ions doped borate and fluoroborate glasses containing lithium, zinc and lead. *Spectrochim. Acta Part A* **2006**, *63*, 276–281. [[CrossRef](#)]
42. Ćirić, A.; Stojadinović, S.; Sekulić, M.; Dramićanin, M.D. JOES: An application software for Judd-Ofelt analysis from  $\text{Eu}^{3+}$  emission spectra. *J. Lumin.* **2019**, *205*, 351–356. [[CrossRef](#)]
43. Haouari, M.; Ben Slimen, F.; Maaoui, A.; Gaumer, N. Structural and spectroscopic properties of  $\text{Eu}^{3+}$  doped tellurite glass containing silver nanoparticles. *J. Alloys Compd.* **2018**, *743*, 586–596. [[CrossRef](#)]
44. Liang, H.; Yang, Z.; Xiao, L.; Xie, F. Radiative transition probability of a europium (III) chelating polymer. *Optoelectron. Adv. Mater. Rapid Commun.* **2010**, *4*, 1396–1399.
45. Bebars, S.; Gadallah, A.S.; Khedr, M.A.; Abou Kana, M.T.H. Photoluminescent properties of the europium and terbium complexes covalently bonded to functionalized mesoporous material PABA-MCM-41. *J. Lumin.* **2017**, *192*, 949–956. [[CrossRef](#)]
46. Kumar, J.S.; Pavani, K.; Babu, A.M.; Giri, N.K.; Rai, S.B.; Moorthy, L.R. Fluorescence characteristics of  $\text{Dy}^{3+}$  ions in calcium fluoroborate glasses. *J. Lumin.* **2010**, *130*, 1916–1923. [[CrossRef](#)]